α-particle knock-on signature in the neutron emission of DT plasmas

L. Ballabio* and G. Gorini†
Department of Physics, University of Milan, I-20133 Milano, Italy

J. Källne
Department of Neutron Research, Uppsala University, S-75121 Uppsala, Sweden

(Received 8 August 1996)

The fast α-particle kinetic effects in fusion plasmas of deuterium and tritium are studied in the perspective that they can give rise to minority populations of fast fuel ions. The resulting modification of the neutron emission spectrum is computed for a plasma in the state of steady thermonuclear burn of conditions similar to those envisaged for the planned ITER tokamak. The nuclear interaction in these scattering α-particle knock-on processes is taken into account explicitly and the dependence on plasma parameters is investigated. The findings provide evidence that neutron spectrometry is a potential diagnostic of the fast α-particle population in burning fusion plasmas. [S1063-651X(97)06602-6]

PACS number(s): 52.40.−w

I. INTRODUCTION

A thermonuclear plasma consists mostly of particles of thermal energies apart from the charged fusion products having energies up to several MeV. In burning deuterium-tritium (DT) plasmas under conditions to be produced in tokamaks such as ITER [1], α particles from the $d+t\rightarrow\alpha+n$ reactions are the most important fusion product. The α particles are slowed down from their creation energy through particle scattering in the plasma, which occasionally is a hard knock-on collision with large energy transfer. The knock-on coupling between the fast α-particle population and the thermal fuel (d and t populations) can generate suprathermal d' and t' populations or similar populations for other ion species in the plasma such as impurities. The knock-on effects on impurities in plasmas have been investigated [2] as a potential α-particle diagnostic through the induced broad, low-intensity feature in the energy spectrum of characteristic photon emission lines. The knock-on effects on fuel ions are of interest because the fusion reactivity would be enhanced by reactions involving the suprathermal populations ($d'+t$ and $t'+d$) compared to the thermal ion reactions only. The $d'+t$ and $t'+d$ reaction rates would normally be small in tokamak plasmas because of the low suprathermal densities ($n_{d'}$ and $n_{t'}$ compared to n_d and n_t) so that the fusion power balance would not be affected. However, the suprathermal densities may be sufficient to give a distinct knock-on signal in the neutron emission spectrum that could be used for the purpose of plasma diagnostics [3]. An initial quantitative study of the knock-on production of d' and t' populations showed that the nuclear scattering amplitude must be considered besides the obvious Coulomb force [4]. This study also suggested that the knock-on effect should be a distinct feature of the neutron emission spectrum that could be observed with high-count-rate and high-sensitivity neutron spectrometers of the magnetic proton recoil type. Other studies have been presented [5] suggesting the use of high-threshold activation techniques.

The purpose of the present work has been to perform an accurate quantitative calculation of the α-particle knock-on effect on the neutron emission spectrum. The best available input information has been used on $\alpha+d$ and $\alpha+t$ scattering in the MeV region in order to determine their contribution to the formation of fast fuel ion populations. In particular, the relative contributions of Coulomb and nuclear scattering have been carefully treated including the interference between the two types of interactions. Since the results showed that the α-particle signature should indeed be detectable, the study was consequently aimed at understanding which diagnostic information can be obtained from the observation of knock-on features. This has been done by demonstrating how sensitive the knock-on signature is to changes in the plasma parameters. The plasma dependence study was performed by including effects previously neglected such as the thermal broadening of the fast ion distributions. The capabilities of this α-particle diagnostic are assessed quantitatively in terms of limiting features such as the attainable statistics of the measurement and time resolution considering also possible interference from other processes in the same energy region of the neutron spectrum.

II. GENERAL APPROACH

The α particles from the $d+t\rightarrow\alpha+n$ fusion reactions are created in the plasma at a characteristic energy of 3.54 MeV with some broadening due to the thermal ion motion. These source α particles are rapidly thermalized in the plasma through small-angle particle collisions as is described by the Fokker-Planck equation [6]. This results in an α-particle population of a certain velocity distribution whose amplitude is given by the equilibrium of the source and slowing down rates for steady-state conditions. Large-angle collisions are rare, but can, on the other hand, impart large energy transfers

*Present address: Department of Neutron Research, Uppsala University, S-75121 Uppsala, Sweden.

†Also at Istituto di Fisica del Plasma, EURATOM, ENEA, CNR Association, I–20133 Milano, Italy.

to the bulk plasma ions. Suprathermal deuterons and tritons (d' and t') can be created in such knock-on collisions and are given an energy that increases with the scattering angle up to the maximum set by E_α; for instance, the maximum energy is $E_{d'}=3.15$ MeV and $E_{t'}=3.47$ MeV for $E_\alpha=3.54$ MeV. The amplitude and energy distribution of the d' and t' source terms are functions of the fast α-particle population.

Large energy transfers require ion interaction at short distance. This means that above a certain energy transfer, the nuclear interaction will come into play. Therefore, the nuclear elastic scattering (NES) cross section must be carefully treated in the calculations of the formation of the d' and t' populations due to α-particle knock-on collisions. The NES contributions either can increase the d' and t' population amplitudes above the level of what pure Coulomb interaction would give or could even lead to a decrease in the case of destructive interference between the two. The $\alpha+d$ and $\alpha+t$ scattering cross sections are also important to know in order to calculate the distribution functions of the d' and t' source terms.

It is clear that the energy integrated densities $n_{d'}$ and $n_{t'}$ will be a very small fraction of the bulk densities. However, the suprathermal ions will have distributions that extend to high energies and there can be the dominant fuel ion component of the plasma even for very low $n_{d'}$ and $n_{t'}$ densities. It is these extreme energy regions that we are interested in here as they can give contributions to the neutron emission spectrum far from the characteristic energy of $E_{n0}=14.02$ MeV. While the bulk ion reactions would give a quasi-Gaussian energy distribution [7] that falls as $\exp[-E_0(\sqrt{E_n}-\sqrt{E_0})^2/C_n]$, with $E_0\simeq E_{n0}$ and $C_n\propto T_i$, where T_i is the ion temperature, the $d'+t$ and $d+t'$ reactions make contributions to the neutron spectrum in the extreme high- and low-energy regions. This means that the signature of the knock-on process is to be found at a certain distance from the 14-MeV peak depending on the $d+t$ fusion reactivity as a function of energy and the magnitude of the knock-on cross sections. The knock-on signature in the neutron emission is calculated in this paper.

III. CROSS SECTIONS

The elastic differential cross section for two zero-spin particles (of mass m_1 and m_2 and charge Z_1 and Z_2 with relative energy E) can be written [8]

$$\frac{d\sigma}{d\Omega}(\theta)=|f_C(\theta)+f'(\theta)|^2 \tag{1}$$

in terms of the Coulomb and nuclear scattering amplitudes $f_C(\theta)$ and $f'(\theta)$. This can be rewritten as the sum of the pure Coulomb cross section $d\sigma_C/d\Omega=|f_C|^2$ and the cross section due to nuclear and interference amplitudes $d\sigma_{\rm NI}/d\Omega=|f'|^2+2|f_Cf'|$ so that

$$\frac{d\sigma}{d\Omega}=\frac{d\sigma_C}{d\Omega}+\frac{d\sigma_{\rm NI}}{d\Omega}. \tag{2}$$

The Coulomb scattering amplitude is given by

$$f_C(\theta)=\frac{n}{2k\,\sin^2(\theta/2)}e^{-in\,\ln\sin^2(\theta/2)+2i\sigma_0} \tag{3}$$

and the nuclear scattering amplitude by

$$f'(\theta)=\frac{1}{2ik}\sum_L\,(2L+1)e^{2i\sigma_L}(e^{2i\delta_L}-1)P_L(\cos\theta). \tag{4}$$

Here $k^2=2m_1m_2E/(m_1+m_2)\hbar^2$, $n=Z_1Z_2\alpha/(v_{\rm rel}/c)$ (the Sommerfeld parameter), $P_L(\cos\theta)$ is the Legendre polynomial of order L, and σ_L and δ_L are phase shifts. The Coulomb phase shifts σ_L are given by

$$\sigma_L=\arg[\Gamma(L+1+in)], \tag{5}$$

where $\arg(Z)$ indicates the angular coordinate of the complex number Z in the complex plane. The nuclear phase shifts δ_L are deduced from experimental data and here we have used results obtained by Mohr *et al.* based on an optical model analysis [9]. For particles with spin $I\neq0$, the cross section takes the form

$$\frac{d\sigma}{d\Omega}=\sum_{M_I}\,\frac{1}{(2I+1)}\sum_{M_I'}\,|f_{M_I'M_I}(\theta,\phi)|^2 \tag{6}$$

with summation over all initial and final spin projections (M_I and M_I') for a given quantization axis. The total scattering amplitudes $f_{M_I'M_I}(\theta,\phi)$ are given by

$$f_{M_I'M_I}(\theta,\phi)=f_C(\theta)\delta_{M_I'M_I}+f'_{M_I'M_I}(\theta,\phi) \tag{7}$$

and the nuclear scattering amplitudes (for quantization direction $\hat{\mathbf{k}}$) are expressed by

$$\begin{aligned}f'_{M_I'M_I}(\theta,\phi)=&\frac{\sqrt{\pi}}{ik}\sum_{L,J}\,\langle LI0M_I|JM_I\rangle\\&\times\langle LIM_I-M_I',M_I'|JM_I\rangle\sqrt{(2L+1)}\\&\times e^{2i\sigma_L}(e^{2i\delta_L^J}-1)Y_L^{M_I-M_I'}(\theta,\phi);\end{aligned} \tag{8}$$

here $\langle ab\alpha\beta|c\gamma\rangle$ are Clebsch-Gordan coefficients and δ_L^J the spin-dependent phase shifts. The nuclear phase shifts determine $d\sigma_{\rm NI}/d\Omega$, while $d\sigma_C/d\Omega$ is readily calculated from the Rutherford formula [Eq. (3)].

For small-angle scattering, the Coulomb term dominates, but this is not important for the generation of fast nuclei. We can assume, without loss of accuracy, that finite contributions to the fast ion populations are only due to collisions with scattering angles $\theta>\theta_{\rm min}$ (in the c.m. frame) or, correspondingly, $\eta_{\rm max}=\cos(\theta_{\rm min})$; as in [10], we chose the limit $\theta_{\rm min}=20^{\rm o}$. Furthermore, since the interference can lead to a negative $d\sigma_{\rm NI}/d\Omega$ value for small angles, a positive value is assured by not allowing $\eta_{\rm max}$ to exceed a certain upper limit (η_0), the value of which can vary with the kinetic energy E of the colliding ions in the c.m. frame. Thus the total (angle-integrated) nuclear-interference (NI) cross section considered for fast ion generation is

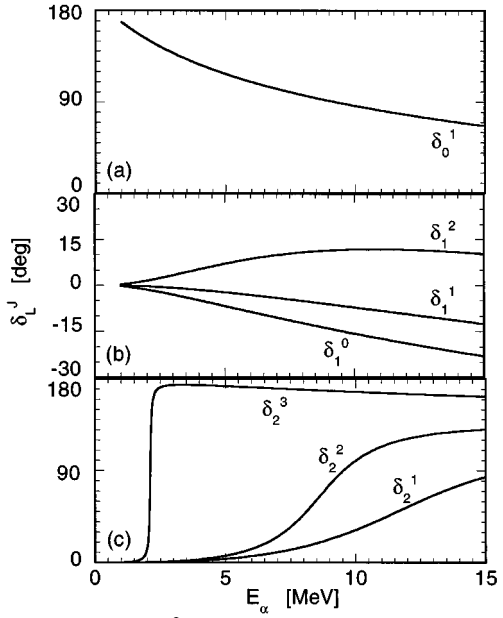

FIG. 1. Phase shifts δ_L^J for $\alpha+d$ elastic scattering of the partial waves $L=0$ (a), 1 (b), and 2 (c) as a function of energy.

$$\sigma_{\mathrm{NI}}(E)=2\pi\int_{-1}^{\overline{\eta}}\frac{d\sigma_{\mathrm{NI}}}{d\Omega}(\eta,E)\,d\eta \tag{9}$$

with $\overline{\eta}=\min(\eta_{\max},\eta_0(E))$. This cross section can be compared with the same integrated Coulomb cross section in order to assess the influence of the nuclear interaction. Moreover, the average cosine of the scattering angle in the laboratory frame is given by

$$\overline{\mu(E)}=\frac{2\pi}{\sigma_{\mathrm{NI}}(E)}\int_{-1}^{\overline{\eta}}\mu(\eta)\frac{d\sigma_{\mathrm{NI}}}{d\Omega}(\eta)\,d\eta, \tag{10}$$

where μ is

$$\mu(\eta)=\frac{m_1+m_2\eta}{\sqrt{m_1^2+2m_1m_2\eta+m_2^2}}, \tag{11}$$

with m_1 and m_2 being the masses of the projectile and target particles, respectively. This can be used as an estimator of the anisotropy of the cross section. As a reference we can use the $\overline{\mu}$ value of an isotropic cross section (in the c.m. system and assuming $m_1>m_2$), which is

$$\overline{\mu_{\mathrm{iso}}}=1-\frac{1}{3}\left(\frac{m_2}{m_1}\right)^2. \tag{12}$$

The total cross sections $\sigma_C(E_\alpha)$ and $\sigma_{\mathrm{NI}}(E_\alpha)$ as well as the average scattering cosine $\overline{\mu(E_\alpha)}$, besides the differential cross sections $d\sigma_{\mathrm{NI}}/d\Omega(\theta,E)$, were calculated using the phase shifts δ_L^J of [9]. The results on σ_C, σ_{NI}, and $\overline{\mu}$ for $\alpha+d$ scattering are shown in Figs. 1 and 2 and for $\alpha+t$ scattering in Figs. 3 and 4; the results on $d\sigma_C/d\Omega(\theta,E_\alpha)$ and $d\sigma_{\mathrm{NI}}/d\Omega(\theta,E_\alpha)$ for $E_\alpha=3.54$ MeV are shown in Figs. 5 and 6.

For $\alpha-d$ scattering it is found that σ_{NI} is generally weakly dependent on E_α, but for a narrow resonance at $E_\alpha\simeq 2.1$ MeV (Fig. 2) due to the behavior of δ_2^3 (Fig. 1);

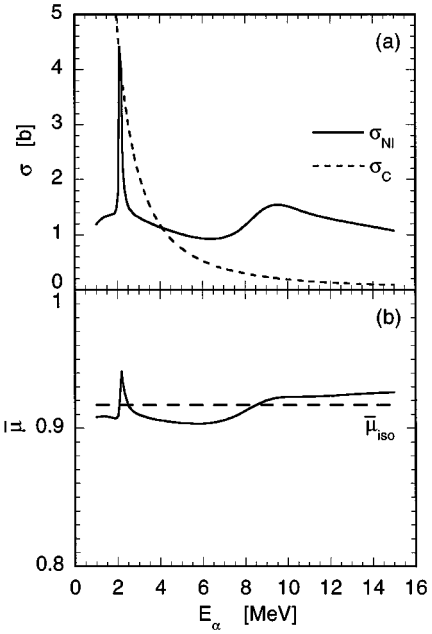

FIG. 2. (a) Total cross sections and (b) average cosine of the scattering angle for elastic $\alpha+d$ scattering as a function of energy. The cross section is divided into contributions of the pure Coulomb interaction (σ_C) and the nuclear interaction plus interference term (σ_{NI}). The average cosine for isotropic scattering ($\overline{\mu_{\mathrm{iso}}}$) is shown for comparison.

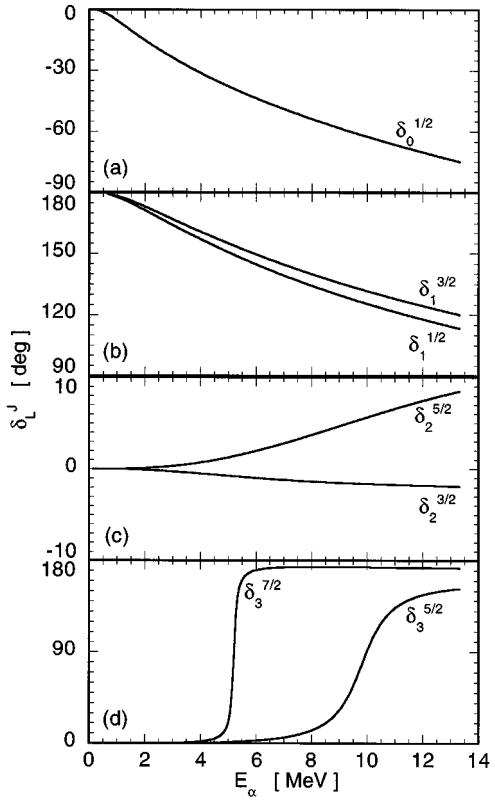

FIG. 3. Phase shifts δ_L^J for $\alpha+t$ elastic scattering of the partial waves $L=0$ (a), 1 (b), 2 (c), and 3 (d) as a function of energy.

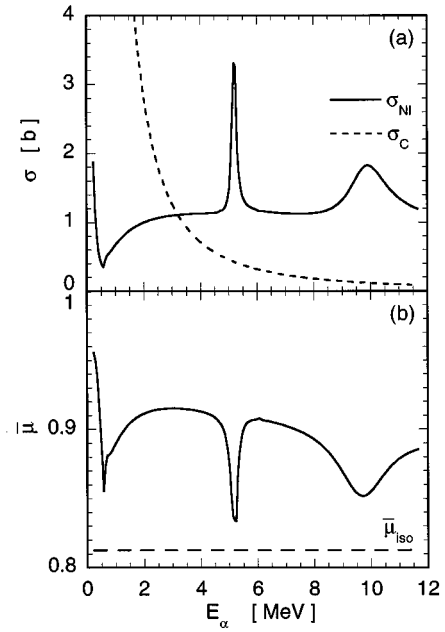

FIG. 4. (a) Total cross sections and (b) average cosine for $\alpha+t$ elastic scattering.

there is also a broad resonance in $\sigma_{\rm NI}$ above 7 MeV due to δ_2^1 and δ_2^2, but it does not concern us here. The 2.1-MeV resonance affects $\alpha-d$ scattering in plasmas as it is located below the α-particle average creation energy $E_{\alpha 0}=3.54$ MeV. The value of $\overline{\mu}$ is near the one expected for an isotropic cross section; the slightly higher value at the resonance indicates a slight preference for forward scattering. The effect of the resonance is to increase the amplitude of the fast deuteron source term over the whole energy range up to the maximum $E_{d'}^{\rm max}=1.87$ corresponding to $E_\alpha=2.1$ MeV. However, since there is some predominance for forward scattering, one can expect the deuteron source term to be correspondingly larger at low energies. Apart from the 2.1-MeV resonance region, the Coulomb term appears to dominate generally the entire region $E_\alpha<4.1$ MeV. This is largely due to the divergence of the Coulomb component at zero energy. However, the differential cross section shows that the NI term actually dominates the limited region of large-angle

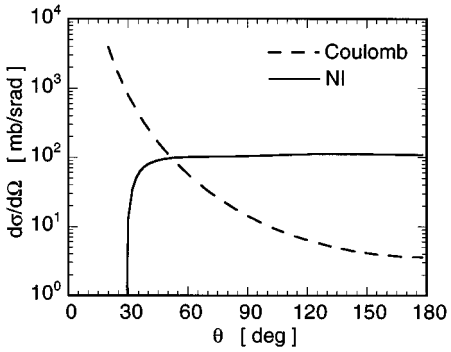

FIG. 5. Differential cross sections for $\alpha+d$ elastic scattering at $E_\alpha=3.54$ MeV. The contributions due to the Coulomb interaction and nuclear interaction plus interference (NI) terms are shown separately.

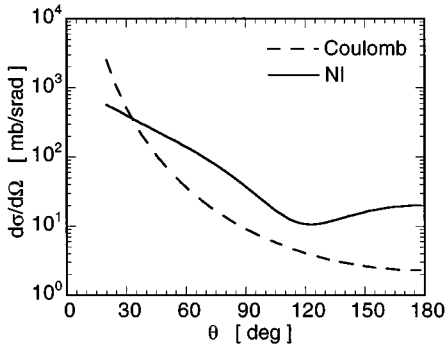

FIG. 6. Differential cross sections for $\alpha+t$ elastic scattering at $E_\alpha=3.54$ MeV.

scattering (viz., $\theta>60°$ of Fig. 6) and this is what contributes the most to the fast ion source term.

There are also resonances in the α-t scattering, but at the relatively high energies of $E_\alpha\simeq 5.2$ MeV and $E_\alpha\simeq 8$ MeV (Fig. 4) (due to the $\delta_3^{7/2}$ and $\delta_3^{5/2}$ terms, Fig. 3). The $\overline{\mu}$ value is larger than typical for isotropic scattering over the entire energy range, implying that forward scattering is favored. The Coulomb term shows an overall dominance in the energy range $E_\alpha<3.2$ MeV (Fig. 4), yet the NI term would dominate the large-angle collisions responsible for fast ion generation.

The present results show that for α-d scattering it is a fair approximation to assume, as was done in [4], that the NI cross section is isotropic and is constant in energy. Only the previously assumed magnitude of $\sigma_{\rm NI}=1.1$ b [11] needs to be adjusted. For α-t scattering, the situation is more complicated, so the calculated results must be used for the NI cross section.

IV. FAST ION POPULATIONS

The slowing down of the fast ions is described by the Fokker-Planck equation for a uniform and thermal DT plasma in a steady state with no spatial diffusion. The equilibrium equation for the velocity distribution $f_Z(v_Z)$ can be written [12] as

$$\frac{1}{v^2}\frac{\partial}{\partial v}(v^3\nu_Z f_Z)=-Q_Z, \tag{13}$$

where Q_Z is the source term for fast nuclei of charge Z and ν_Z is the collision frequency. For a plasma of several ion species Z_j besides the electrons, the contribution to ν_Z is

$$\nu_Z=\sum_j \nu_{Zj}, \tag{14}$$

where

$$\nu_{Zj}=\frac{4\pi Z^2 Z_j^2 e^4 n_j \Lambda_{Zj}}{m_Z m_j v^3}\left[\Phi(y)-\frac{2}{\sqrt{\pi}}ye^{-y^2}\right]. \tag{15}$$

Here the velocity is expressed relative to the thermal ion speed by the parameter $y=v/v_{{\rm th}j}$; $\Phi(y)$ is the error function

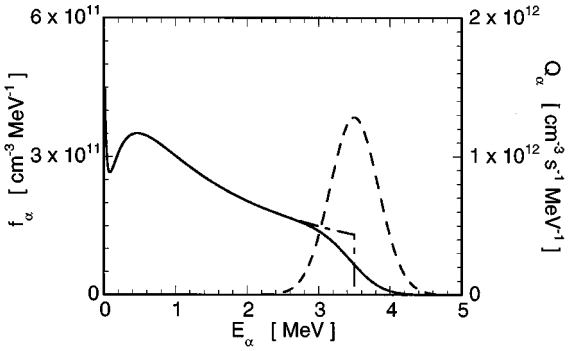

FIG. 7. Energy distribution function f_α (solid line) and source term Q_α (dashed line) of α particles in a plasma of reference conditions. Also shown is the $\tilde{f}_\alpha$ function corresponding to a monoenergetic source term (dash-dotted line).

$$\Phi(y)=\frac{2}{\sqrt{\pi}}\int_0^y e^{-x^2}dx, \tag{16}$$

and Λ_{Zj} is the Coulomb logarithm

$$\Lambda_{Zj}(v)=\ln\sqrt{\frac{T_j}{\pi n_e}}\frac{\mu}{e\hbar}\max\left(v,\frac{2}{\pi}v_{\mathrm{thj}}\right). \tag{17}$$

The slowing down in the plasma is mostly due to multiple small-angle Coulomb scattering (see, e.g., [6]) while, for instance, nuclear scattering is negligible (see Figs. 5 and 6 above).

The slowing-down calculations were performed for a plasma with parameters representative of the ITER tokamak, i.e., electron and ion temperatures of $T_e=T_i=20$ keV and an electron density of $n_e=10^{14}$ cm^{-3}. Moreover, deuteron and triton densities of $n_d=n_t=\frac{1}{2}n_e$ have been assumed, implying a plasma free of impurities ($Z_{\mathrm{eff}}=1$).

The results for α particles are shown in Fig. 7, where one can compare the slowing-down energy distribution f_α with its source term Q_α of finite temperature ($T_i=20$ keV). The source term $Q_\alpha(E_\alpha)$ is given by the d-t fusion reactions. If $T_i=0$, the source term would be monoenergetic (i.e., $E_\alpha=E_\alpha^*=3.54$ MeV) with the energy distribution function $\tilde{f}_\alpha$ given by the analytical expression

$$\tilde{f}_\alpha(\mathbf{v}_\alpha)=\frac{n_d n_t\langle\sigma v\rangle}{4\pi v_\alpha^3\nu_\alpha}\times\begin{cases}1, & v_\alpha\leq v_\alpha^*\\ 0, & v_\alpha>v_\alpha^*,\end{cases} \tag{18}$$

where $v_\alpha^*=\sqrt{2E_\alpha^*/m_\alpha}$ [13,2]. This is shown in Fig. 7 as a dot-dashed curve over the energy region from 2.5 to 3.5 MeV. For finite temperatures, the α-particle distribution must be calculated numerically. The result is shown in Fig. 7 as a continuous curve. The analytical expression is thus accurate for the low-energy region, while the numerical approach must be used to obtain the correct shape in the high-energy region. The analytical approach works for energies up to $E_\alpha\simeq 2.5$ MeV, which is the lower limit of the α-particle creation energy for the case $T_i=20$ keV considered. In this region, the f_α distribution is dependent only on the integrated amplitude of the source term, for steady-state conditions, regardless of its energy distribution.

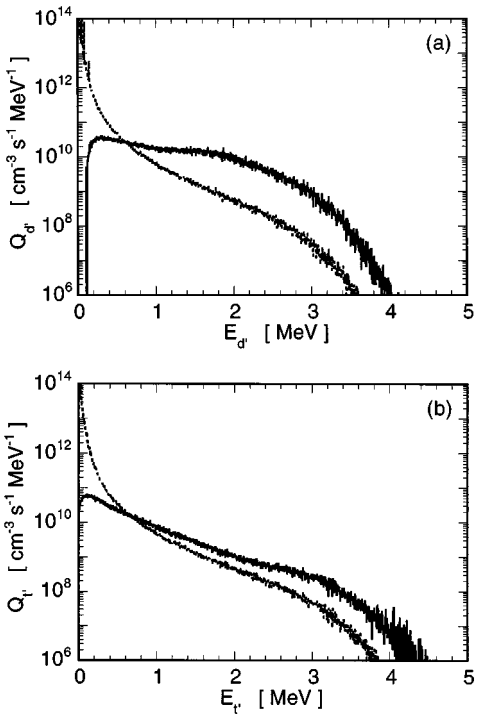

FIG. 8. Source term functions $Q_{d'}$ and $Q_{t'}$ of (a) fast deuterons and (b) tritons due to α-particle knock-on collisions. The Coulomb (dotted line) and NI (solid line) contributions are shown separately.

For cold plasmas ($T_i=0$) one can use the analytical expression for f_α [Eq. (18)] to describe the d' and t' source terms, which can be written [13,2]

$$Q_{i'}(v_{i'})=\frac{8\pi\gamma^2 n_i}{v_{i'}}\int_{\gamma v_{i'}}^{\infty}\frac{d\sigma}{d\Omega}\tilde{f}_\alpha(v_\alpha)v_\alpha dv_\alpha, \tag{19}$$

where $\gamma=(m_i+m_\alpha)/2m_\alpha$ and $d\sigma/d\Omega=d\sigma_C/d\Omega+d\sigma_{\mathrm{NI}}/d\Omega$. The effect of temperature on the fast ion source term can be included in numerical calculations, which were done with the Monte Carlo code CRASHTEST [14]. This also allowed the use of the NI cross sections in tabulated form as well as the separation between contributions from σ_{NI} and σ_C. In order to avoid zero-energy divergences, low-energy cutoffs at $E=T_i$ were adopted for E_d and E_t. The results on $Q_{d'}(E_{d'})$ and $Q_{t'}(E_{t'})$ are shown in Fig. 8. It can be seen that the NI term is dominant for ion energies above $E_{d'}\simeq 0.6$ MeV and $E_{t'}\simeq 0.65$ MeV, which is most pronounced for $Q_{d'}$. This difference also reflects the relative NI strength between $Q_{d'}$ and $Q_{t'}$ since the Coulomb cross sections are the same except for a minor kinematic effect. The low-energy NI source terms show differences, which is not surprising as the phase shifts are quite different for $\alpha+d$ and $\alpha+t$; in particular, the latter ones change rather rapidly as one approaches $E_\alpha\rightarrow 0$ and this will dominate the $E_i\rightarrow 0$ behavior (cf. Figs. 3 and 1).

The source terms $Q_{d'}$ and $Q_{t'}$ are used in Eq. (13), which is solved numerically to determine the population functions $f_{d'}$ and $f_{t'}$ (Fig. 9). It can be seen that there are some differences between the d' and t' distributions. The $Q_{t'}$ amplitude is stronger than $Q_{d'}$, except for the high-energy tail. Both suprathermal populations are significantly different

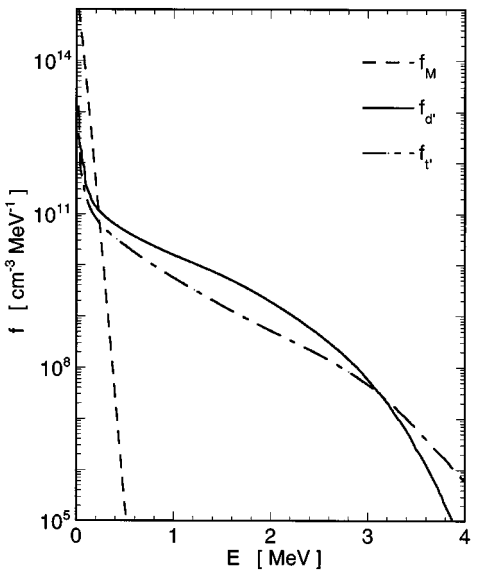

FIG. 9. Energy distribution functions for steady-state populations of fast deuterons ($f_{d'}$) and tritons ($f_{t'}$). The Maxwellian distribution f_M of thermal ions ($T_i=20$ keV) is shown for comparison.

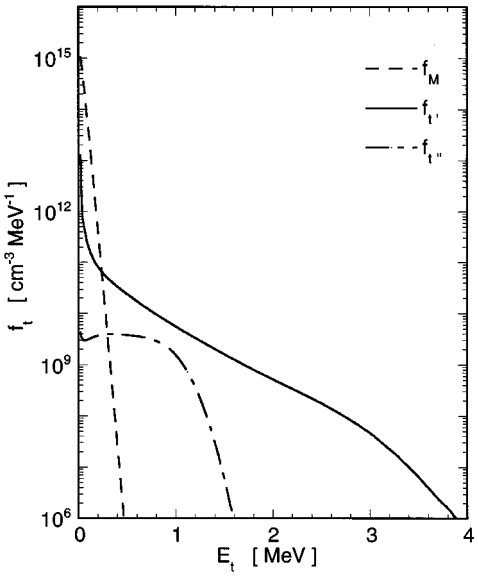

FIG. 10. Comparison of distribution functions of steady-state fast triton populations due to α-particle knock-on ($f_{t'}$) and triton burn-up ($f_{t''}$). The Maxwellian distribution function f_M is also shown.

from the Maxwellian distribution of the bulk ions (also shown in Fig. 9) and they both dominate for $E>0.2$ MeV. The truncation at $E=T_i=20$ keV therefore has no influence on the high-energy part. The fast ion components are weak and can be estimated by the relative density ratios $n_{d'}/n_d=0.4\%$ and $n_{t'}/n_t=0.3\%$ considering the region $E>E$. Therefore, the neutron production by reactions involving two fast ions is negligible relative to those between fast and thermal ions. Only the latter need to be considered.

Finally, we note that another intrinsic source of suprathermal ions in DT plasmas, which can produce fusion neutrons, is the reaction $d+d\rightarrow p+t_{dd}$ ($t_{dd}\equiv t''$). The characteristic energy of this source term is $E_{t''0}\simeq 1$ MeV and is calculated to have the slowing-down distribution $f_{t''}$ shown in Fig. 10. The t'' distribution is of smaller amplitude than that of $f_{t'}$; the ratio is always smaller than 1/6 (reached at $E=0.8$ MeV), while for the interesting region of higher energies ($E>1.2$ MeV) it is vanishingly small. Therefore, the neutron spectrum due to $d'+t$ and $d+t'$ reactions reflecting plasma knock-on effects can normally be observed without interference from the so-called triton burn-up contribution.

V. NEUTRON EMISSION SPECTRUM

The fusion neutron energy is determined (nonrelativistically in the c.m. system) by [15,16]

$$E_n=\frac{m_\alpha}{m_n+m_\alpha}(Q+K)+V_{\text{c.m.}}\cos\theta\sqrt{\frac{2m_nm_\alpha}{m_n+m_\alpha}(Q+K)}+\frac{1}{2}m_nV_{\text{c.m.}}^2 \tag{20}$$

in terms of the c.m. system velocity ($\mathbf{V}_{\text{c.m.}}$), the angle θ between $\mathbf{v}_n$ and $\mathbf{V}_{\text{c.m.}}$, the reaction Q value, and the total incident kinetic energy ($K=\frac{1}{2}\mu v_{\text{rel}}^2$); $\mu=m_dm_t/(m_d+m_t)$ is the reduced mass and $\mathbf{v}_{\text{rel}}$ the relative velocity of the reacting particles. For a fast incident particle i (being d' or t') on a stationary target (being t or d), the neutron energy varies within the bounds set by $\theta=0°$ and 180° depending on the incident ion energy (E_i); Fig. 11 shows that $E_n^{\max}(E_i)$ for $\theta=0°$ approaches 20 MeV for deuterons and tritons of 3 MeV. The neutron energy distribution is constant between the extreme limits $E_n^{\min}$ and $E_n^{\max}$ (''square box'' shape, S_c) for fast monoenergetic ions impinging isotropically on a cold target. If instead the target consists of thermal ions, the distribution will modify the square box shape into one with smoothed edges (S_{th}). For ions with distribution function $f_{i'}$, the spectrum can be written

$$\frac{dN}{dE}(E_n)=\int f_{i'}\sigma_{i'i}v_{i'}S_{\text{th}}(E_n;v_{i'},T_i)dv_{i'}, \tag{21}$$

while the total neutron yield is

$$Y'=\int f_{i'}\sigma_{i'i}v_{i'}dv_{i'}. \tag{22}$$

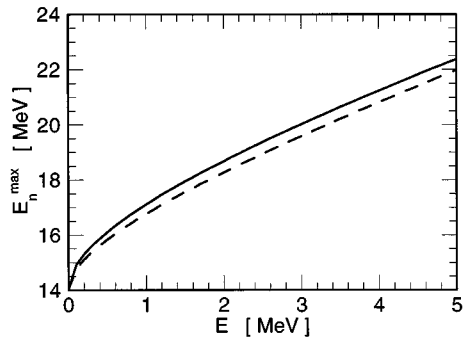

FIG. 11. Maximum neutron energy $E_n^{\max}$ of the reaction $t'+d\rightarrow\alpha+n$ (solid line) and $d'+t\rightarrow\alpha+n$ (dashed line) as a function of energy ($E=E_{t'}=E_{d'}$).

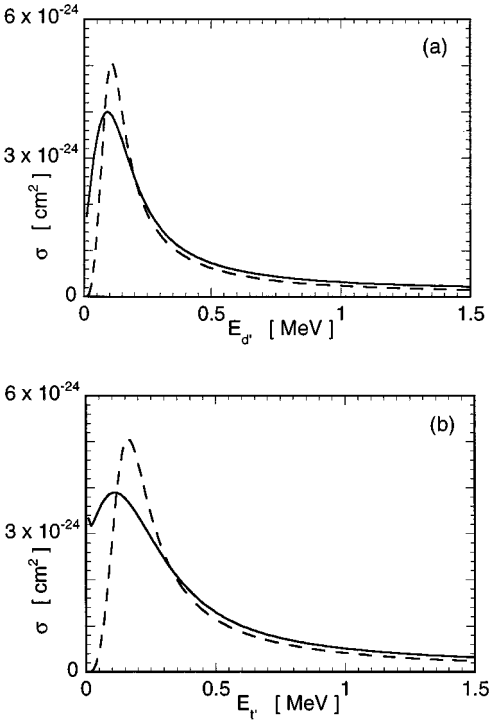

FIG. 12. Cross section of the (a) $d'+t\rightarrow\alpha+n$ and (b) $t'+d\rightarrow\alpha+n$ reactions as a function of energy for target ions that are thermal ($T_i=20$ keV, solid lines) and cold ($T_i=0$, dotted lines).

Here $\sigma_{i'i}$ is the thermal cross section defined as $\sigma_{i'i}(v_{i'},T_i)=\langle\sigma v\rangle(T_i)/v_{i'}$, where $\langle\sigma v\rangle$, is the reactivity, i.e., neutron yield per pair of reacting ions where one is monoenergetic and the other belongs to a thermal distribution. We have calculated the energy dependence of the thermal cross section for $d'+t$ and $d+t'$ reactions and compared the results with available information on the corresponding regular (cold) cross section (Fig. 12). We note that the thermal effect moderates the maximum of the cold cross section occurring at $E_{d'}\simeq 100$ keV and $E_{t'}\simeq 150$ keV for $d'+t$ and $d+t'$. This means that the thermal cross section is increased at low and high energies relative to the cold one, which is most conspicuous on the low-energy side. The peak position is thus shifted to lower energy.

Neutron energy spectra were calculated with the Monte Carlo method using the APACHE code [14]. The code samples the deuteron and triton velocity distributions, thus simulating single reactions occurring at specific values of relative ion energy. All such events were treated statistically and assigned appropriate weights including the calculated reaction cross section. The cross-section parametrization of [17] and the angular differential cross section of [18] were used. The sampling method was administered so as to provide good statistics also in energy ranges where the spectrum amplitude is down by many orders of magnitude relative to the peak value. The results show that the neutron emission spectrum of a burning plasma consists of two components due to thermal and suprathermal ion reactions (Fig. 13). The suprathermal component has low- and high-energy tails that extend well beyond the region dominated by the thermal ion reactions. The middle region around $E_n=14$ MeV appears as a flat level, but this is just an artifact reflecting the adopted

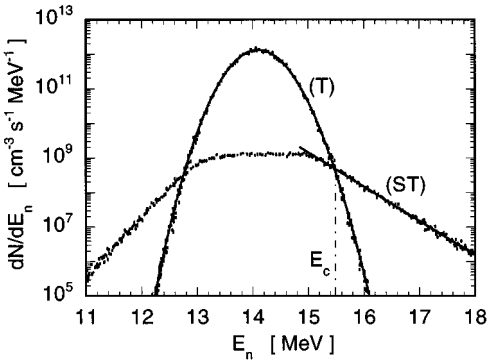

FIG. 13. Neutron energy spectra due to suprathermal (ST) ion reactions ($d'+t$ and $t'+d$) with exponential fit to the high-energy tail compared with thermal (T) ion reactions ($d+t$) with a quasi-Gaussian curve fit. The crossover point (E_c) of the two spectra is indicated. The calculations represent steady-state plasma conditions for a temperature of $T_i=T_e=20$ keV, as explained in the text.

truncation using $f_{d'}=f_{t'}=0$ for $E_{d'}=E_{t'}<E_{\min}=150$ keV in the calculations. The important feature here, however, is that there exist regions where the suprathermal component dominates the spectrum. For the plasma conditions considered, these regions are defined by the upper and lower bounds $E_C=12.7$ and 15.5 MeV. Note that these limits depend weakly on the assumed T_i value reflected in the width of the thermal component. The low-energy region cannot be observed experimentally due to high background so only the high-energy tail can be used to measure the suprathermal component. The region $E_n>15.5$ MeV represents an integrated amplitude yield (Y'), which is a fraction of the total yield (Y) at the level of $Y'_{\rm rel}=1/5000$. The useful α-particle knock-on signal is thus a weak feature of the neutron emission spectrum for reference plasma conditions.

VI. α-PARTICLE INFORMATION

The neutron spectrum can be described in terms of a Gaussian thermal component and a suprathermal component (Fig. 13). The latter, considering only the high-energy part, can be analyzed as an exponential given by two parameters, namely, the yield Y' and the slope factor λ. The yield Y' is defined as

$$Y'=\int_{E_C}^{\infty}\frac{dN}{dE_n}dE_n\,. \tag{23}$$

From the results in Fig. 13 one determines $Y'_{\rm rel}=0.021\%$ or, after subtracting the thermal component near E_C, $Y'_{\rm rel}=0.018\%$. The slope factor λ is defined through

$$\frac{dN'}{dE_n}\simeq\frac{Y'}{\lambda}e^{-(E_n-E_C)/\lambda}, \tag{24}$$

which in practice is obtained by fitting an exponential to the spectrum in the range $E_n>E_C$. This gives $\lambda=0.44$ MeV.

The quantities $Y'_{\rm rel}$ and λ are dependent on the plasma parameters, e.g., the temperature T_e. It should be noted that $Y'_{\rm rel}$ is independent of the reactivity $\langle\sigma v\rangle$, so that no T_i dependence is introduced this way. With the local (around a

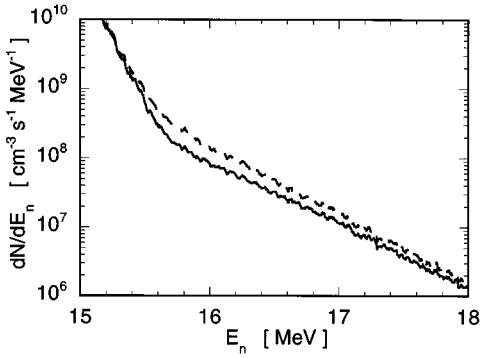

FIG. 14. Energy spectrum for the neutron emission from a burning plasma in steady-state conditions without (dashed line) and with an extra α-particle loss mechanism (solid line), as explained in the text.

certain temperature) approximation $Y'_{\rm rel}\propto T_e^{a_Y}$, one obtains $a_Y=3.3$ for $T_e=20$ keV. The dependence on other parameters such as the ion densities n_d and n_t and the effective charge $Z_{\rm eff}$ is found to be weaker. The plasma dependence of $Y'_{\rm rel}$ can be described by [14]

$$Y'_{\rm rel}\propto T_e^{a_Y}\frac{n_d n_t}{n_e^2}=T_e^{a_Y}\left(\frac{Z-Z_{\rm eff}}{Z-1}\right)^2\frac{n_d/n_t}{(1+n_d/n_t)^2}, \qquad (25)$$

where Z is the charge of the main impurity element. A similar analysis for the slope factor λ gives with the approximation $\lambda\propto T_e^{a_\lambda}$ an estimated value of $a_\lambda=0.14$ for $T_e=20$ keV; i.e., λ is practically insensitive to changes in plasma parameters. On the other hand, changes in the suprathermal ion population would affect $Y'_{\rm rel}$ and λ rather directly, which would therefore reflect the plasma confinement properties. It is therefore interesting to investigate the response of the neutron emission spectrum to changes in the d', t', and α populations.

For the purpose of illustration, we consider a situation where the confinement is affected by a specific loss mechanism such as where all α particles of energy $E_\alpha<E_0$ are suddenly lost. The corresponding α-particle distribution function takes the form

$$\tilde{f}_\alpha=f_\alpha\times\begin{cases}0, & E_\alpha<E_0\\ 1, & E_\alpha\geqslant E_0,\end{cases} \qquad (26)$$

where f_α is the unperturbed distribution. For $E_0=2$ MeV one obtains a change in the neutron spectrum that amounts to $\Delta Y'/Y'=-40\%$ and $\delta\lambda/\lambda=+13\%$ (Fig. 14). This means that by measuring $Y'_{\rm rel}$ and λ one cannot only verify the presence of α particles in the plasma, but also monitor more substantial changes in the α-particle population. Generally, the plasma confinement properties and the onset of extra loss mechanisms would be investigated quantitatively on the basis of comparison of Y' and λ values obtained from measurements and plasma model predictions.

To examine the specific diagnostic information in $Y'_{\rm rel}$ and λ, we introduce the quantity $P_\alpha(E_\alpha)$ expressing the probability for an α-particle of energy E_α to contribute to Y'. This probability can be divided according to type of reaction

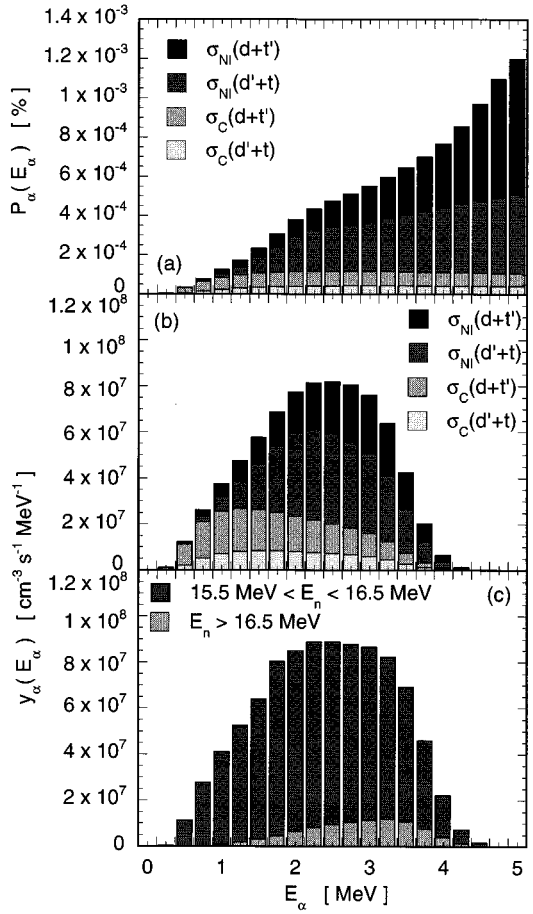

FIG. 15. (a) Probability $P_\alpha(E_\alpha)$ for α-particle knock-on contribution to a suprathermal neutron signal with energy $E_n>E_C$ and (b) and (c) differential yield $y_\alpha(E_\alpha)$ of knock-on neutron production as a function of α-particle energy. A distinction is made between different reaction contributions [in (a) and (b)] and different neutron energy ranges [in (c)]. See the text for definitions.

$(d+t'$ or $d'+t)$ and interaction (NI or Coulomb), i.e., the fusion reaction cross sections $\sigma_{\rm NI}(d+t')$, $\sigma_{\rm NI}(d'+t)$, $\sigma_C(d+t')$, and $\sigma_C(d'+t)$. The differential neutron yield $y_\alpha(E_\alpha)=dY'/dE_\alpha=f_\alpha(E_\alpha)P_\alpha(E_\alpha)$ is also of interest in this context for which we make the same cross-section decomposition while also distinguishing between the regions of 15.5 MeV$<E_n<$16.5 MeV and $E_n>$16.5 MeV. The calculated results on $P_\alpha(E_\alpha)$ and $y_\alpha(E_\alpha)$ are shown in Fig. 15.

First, it is interesting to note that $P_\alpha(E_\alpha)$ increases with E_α [Fig. 15(a)] and that Y' is the integrated product of the α-population distribution and the probability P_α, i.e.,

$$Y'=\int f_\alpha P_\alpha dE_\alpha. \qquad (27)$$

With the approximation $P_\alpha(E_\alpha)\propto E_\alpha$, one obtains

$$Y'\propto\int f_\alpha E_\alpha dE_\alpha, \qquad (28)$$

where the integral is the fast α-particle pressure in the plasma p_α, i.e., $Y'=Cp_\alpha$. Neutron spectrometry is thus a potential diagnostic for the α-particle pressure, but the determination of the proportionality factor C depends on input

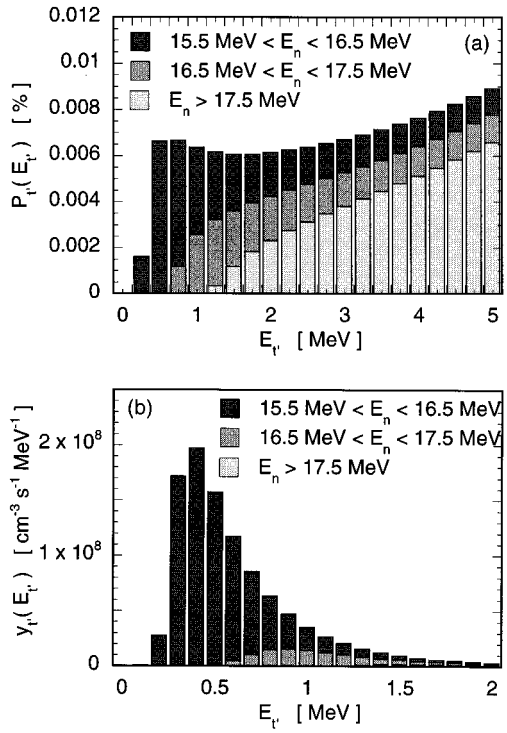

FIG. 16. (a) Probability $P_{t'}(E_{t'})$ for the fast triton contribution to the suprathermal neutron signal and (b) neutron differential yield $y_{t'}(E_{t'})$ as a function of triton energy with a distinction made with respect to the different neutron energy range.

information from other diagnostics. Moreover, the knock-on cross section must also be known.

The results of Fig. 15(a) show that the probability for the knock-on process to contribute to the fast neutron production is crucially dependent on the nuclear interaction. Indeed it dominates over the Coulomb contribution for α energies of above 1.5 MeV, which is also true if one takes into account the f_α distribution function [Fig. 15(b)]. The inclusion of the nuclear interaction is therefore essential and its relative strength is important for the magnitude of Y', but also for the shape (λ). The latter derives from the observation in Fig. 15(c) that there is a certain correlation between E_α and E_n so that, for instance, the region $E_n > 16.5$ MeV is mostly fed by high-energy α particles.

The sensitivity of the neutron spectrum to details of the d' and t' distributions can be studied in a similar way. For instance, calculations of the quantities $P_{t'}(E_{t'})$ and $y_{t'}(E_{t'})$ for the t' distribution give the results on $P_{t'}(E_{t'})$ and $y_{t'}(E_{t'})$ shown in Fig. 16 for three different neutron energy regions. It can thus be observed that the low- and high-energy regions of the neutron spectrum are mostly fed by tritons of low and high energies, while the intermediate-energy region draws contribution more evenly from tritons of different regions [Fig. 16(a)]. A closer energy correlation between the neutrons and tritons is shown if one considers also the $f_{t'}$ distribution function of the plasma [Fig. 16(b)]. The difference between $y_{t'}$ and y_α [Figs. 15(c) and 16(b)] is a reflection of the underlying features of the distribution functions where $f_{t'}$ shows a much stronger decrease with energy than f_α.

The model used in this work can be refined by taking into account the plasma in-homogeneity, which is neglected here. In fact, the α particles and the fast nuclei involved in the generation of suprathermal neutrons describe orbits in the plasma along which the values of the plasma parameters change. Similarly, the neutron spectra observed will be a superposition of contributions from plasma regions of different temperature and density. These effects are estimated to be small, but could weakly modify the results.

VII. EXPERIMENTAL CONSIDERATIONS

Observation of the α-particle knock-on effects in the neutron emission requires a neutron spectrometer with high sensitivity. This means, first of all, that it must have sufficient efficiency so that the signal can be measured with desired count rate (C_n). Moreover, it is desired that the weak knock-on signal and the dominant (''thermal'') peak of the neutron emission be measured simultaneously. This, in turn, implies requirements on the minimum acceptable values of count rate capability ($C_n^{\rm cap}$) and energy coverage ($\Delta E_C/E$). With a target signal count rate of 1000 s^{-1}, one obtains $C_n^{\rm cap} > 10^7$ s^{-1}, while $\Delta E_C/E$ should exceed $\pm 20\%$.

The sensitivity must also include the ability to handle the potential interference from background. The background affecting neutron spectrometry is essentially of two types: (i) ambient background that can affect any part of the neutron spectrum and (ii) background that arises from the fact that neutrons emitted from the plasma can reach the spectrometer after having scattered in surrounding material including the walls of the collimator through which the plasma is viewed; the scattered background reflects the direct emission spectrum but for a downshift in energy (depending on the detailed conditions for the scattering). The spectrometer should have such properties that the background can be kept below the level where it interferes with the observation of the signal spectrum, i.e., without having to apply background subtraction to the data acquired. This is possible only for the high-energy part of the knock-on signal as the scattering background on the low-energy side of the thermal peak is an irreducible part of neutron spectral measurements and can only marginally be controlled by change of the experimental conditions with existing practical constraints [19]. A schematic representation of the background components connected with measurement of the neutron emission spectrum over seven orders of magnitude in the energy region 12–20 MeV is shown in Fig. 17.

One possible choice of instrument for this application is the magnetic proton recoil (MPR) spectrometer [20,21]. It is estimated to be able to satisfy the above requirements on background control (cf. Fig. 17), count rate capability, and energy coverage. The neutron flux efficiency factor of the MPR is $\varepsilon \simeq 10^{-4}$ cm^2, which could give a count rate of up to about 10^3 s^{-1} for the high-energy tail of the knock-on spectrum for a typical ignited discharge in ITER (fusion power of about 1 GW). This measurement would give statistical errors as illustrated in Fig. 18 with regard to measuring the slope factor λ using a data accumulation (resolution) time of $\Delta t = 1$ s. With this time resolution it is only possible to determine the intensity of the knock-on spectrum while the statistics would only allow the λ parameter to be determined with an accuracy of only 30%. This means, for instance, that

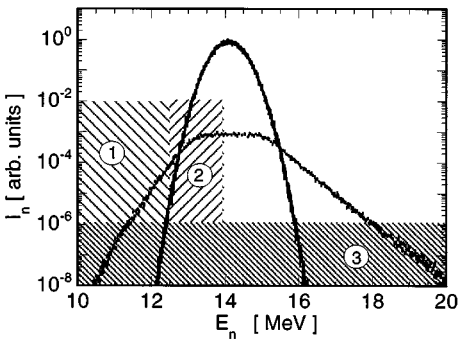

FIG. 17. Schematics of the neutron spectrum in a collimated tokamak experiment due to emission from the plasma (signal) and background due to scattered neutrons (1+2) and ambient radiation (3).

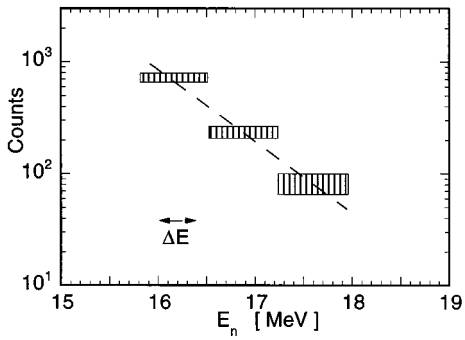

FIG. 18. Illustration of how data on the high-energy tail of the neutron spectrum due to α-particle knock-on can be used based on the assumption of 1000 counts. Energy bins and statistical errors for each bin are shown. ΔE indicates the spectrometer intrinsic resolution.

one cannot measure changes in losses of α particles in the plasma over short time periods. On the other hand, one can monitor the plasma conditions where, for instance, there is a distinct change from one loss level to another. Thus a λ measurement over integral times of 1–10 s has a diagnostic value, as it can be used to compare with plasma model predictions and to confirm the presence of α particles as one approaches the ignition state. It is also interesting to note that over time periods of tens of seconds, one can obtain an accuracy at the 10% level in the λ determination. ''Steady-state'' changes in the plasma that show up in the neutron spectrum can therefore be monitored at the 10% sensitivity level over $\Delta t \geqslant 10$ s, which is of interest over burn times of thousands of seconds.

VIII. CONCLUSION

We have calculated the knock-on rate for collisions between α particles (from $d+t \rightarrow \alpha+n$) and fuel ions (d and t) in deuterium-tritium plasmas of steady-state ignition conditions in order to determine the neutron spectrum resulting from reactions involving fast deuteron (d') and triton (t') populations, i.e., $d'+t \rightarrow \alpha+n$ and $d+t' \rightarrow \alpha+n$. It is found that the nuclear interaction of the $\alpha+d$ and $\alpha+t$ large-angle scattering changes both the magnitude and shape of the d' and t' populations compared to what pure Coulomb scattering would give. Therefore, both the nuclear and Coulomb interaction must be included explicitly in the description of large-angle scattering at energies of plasma ions, i.e., $E_\alpha \leqslant 3.5$ MeV (but whose half amplitude edge is raised by the thermal ion motion, e.g., by 23% to 4.3 MeV at $T_i = 20$ keV). The calculated neutron spectra of $d'+t$ and $t'+d$ are found to dominate over that of $d+t$ for energies of $E < E_0 - \Delta E$ and $E < E_0 + \Delta E$, where $E_0 = 14$ MeV and ΔE is determined to be 1.5 MeV for planned ignition plasmas in tokamaks such as ITER. The high-energy knock-on signal is predicted to have an amplitude of 0.02% relative to the main neutron signal of $d+t$ reactions. An analysis of the information content in the signal suggests that it can be used as a monitor of the α-particle population in fusion plasmas. The measured amplitude and shape of the neutron knock-on spectrum can be used to study the confinement properties of the plasma including effects of fast ion loss mechanisms, while quantitative results would be based on a comparison of measurements with plasma model predictions. It was shown that the amplitude is proportional to the fast α-particle pressure in the plasmas. Finally, the measurability of the knock-on signature in the neutron spectrum was assessed based on presently known experimental techniques. It is found that a neutron spectrometer of the magnetic proton recoil type satisfies the feasibility requirements both with regard to the absolute signal intensity giving sufficient count rate and relative to examined background sources. It is concluded that neutron spectrometry is a potential α-particle diagnostic method to monitor the fast ion confinement properties of ignition plasmas in tokamaks and to measure the α-particle pressure. The present findings are relevant for the planning of future ignition plasma experiments on, for instance, ITER as well as for attempting the first preliminary observations during the preignition studies to be performed on the Joint European Torus.

ACKNOWLEDGMENTS

We gratefully acknowledge Professor P. Mohr and G. Staudt for kindly providing the phase shift data and the code for the calculation of the nuclear scattering cross sections. This work was supported by the Swedish Natural Science Research Council (NFR), the Gustafsson Foundation, and EURATOM.

[1] R. Parker, in *Diagnostics for Experimental Thermonuclear Fusion Reactors*, edited by G. Gorini, P.E. Stott, and E. Sindoni (Plenum, New York, 1996), p. 1.

[2] P. Helander, M. Lisak, and D. D. Ryutov, Plasma Phys. Control. Fusion **35**, 363 (1993).

[3] J. Källne and G. Gorini, Fusion Technol. **25**, 341 (1994).

[4] G. Gorini, L. Ballabio, and J. Källne, Rev. Sci. Instrum. **66**, 936 (1995).

[5] R. Fisher, P. B. Parks, J. M. McChesney, and M. N. Rosenbluth, Nucl. Fusion **34**, 1291 (1994).

[6] N. Krall and A. Trivelpiece, *Principles of Plasma Physics* (McGraw-Hill, New York, 1973).
[7] L. Ballabio, G. Gorini, and J. Källne, Rev. Sci. Instrum. (to be published).
[8] G. Satchler, *Direct Nuclear Reactions* (Oxford University Press, New York, 1983).
[9] P. Mohr *et al.*, Phys. Rev. C **48**, 1420 (1993).
[10] S. Perkins and D. Cullen, Nucl. Sci. Eng. **77**, 20 (1981).
[11] K. Brueckner and H. Brysk, J. Plasma Phys. **10**, 141 (1973).
[12] B. Trubnikov, Rev. Plasma Phys. **1**, 105 (1965).
[13] D. Ryutov, Phys. Scr. **45**, 153 (1992).
[14] L. Ballabio, Uppsala University Neutron Physics Report No. UU-NF 95#7, 1995 (unpublished).
[15] H. Brysk, Plasma Phys. **15**, 611 (1973).
[16] W. Heidbrink, Nucl. Instrum. Methods Phys. Res. Sect. A **236**, 380 (1985).
[17] H.-S. Bosch and G. Hale, Nucl. Fusion **32**, 611 (1992).
[18] H. Liskien and A. Paulsen, Nucl. Data Tables **11**, 569 (1973).
[19] P. Antozzi *et al.*, Nucl. Instrum. Methods Phys. Res. Sect. A **368**, 457 (1996).
[20] J. Källne and H. Enge, Nucl. Instrum. Methods Phys. Res. Sect. A **311**, 595 (1992).
[21] J. Källne *et al.*, in *Diagnostics for Experimental Thermonuclear Fusion Reactors*, edited by G. Gorini, P.E. Stott, and E. Sindoni (Plenum, New York, 1996), p. 397; G. Ericsson *et al.*, *ibid.*, p. 413.